Influence of Gain Saturation, Gain Asymmetry, and Pump/Probe Depletion on Wavelength Conversion Efficiency of FWM in Semiconductor Optical Amplifiers

N. C. Kothari and Daniel J. Blumenthal, *Member, IEEE*

Abstract— **The effects of gain saturation, gain asymmetry, and pump/probe depletion on the conversion efficiency of four-wave mixing (FWM) in semiconductor optical amplifiers are studied analytically and numerically. The power dependence of FWM coupling coefficients and ultrafast relaxation-related gain mechanisms are included in the model. By studying the FWM efficiency in the transition from unsaturated to strongly saturated regions, it is seen that gain asymmetry results in deviation from small-signal models when the pump-probe detuning and pump powers are small. At high pump injection or gain conditions, it is also shown that the small-signal model breaks down even for relatively large detuning frequencies. Probe depletion is also seen to be critical under saturated conditions and an upper bound is derived for ranges of input pump power, pump-probe detuning, and gain for a given amplifier under which the small-signal model is valid.**

I. Introduction

NONDEGENERATE four-wave mixing (FWM) in traveling-wave semiconductor optical amplifiers (SOA's) has been studied for frequency conversion and dispersion compensation in wavelength division multiplexed fiber-optic networks. The FWM frequency-conversion process in SOA's is transparent to modulation rate and format, can be used to convert multiple wavelengths simultaneously [1], [2], and is efficient over large frequency ranges [3]–[5]. The conversion efficiency under general saturation conditions were investigated in [6] neglecting pump and probe depletion and gain asymmetry. In [7], pump and probe depletion were accounted for by considering four coupled nonlinear wave equations for the pump, probe, and two signals. Carrier density modulation limited the maximum detuning frequencies for this model to approximately 10 GHz. Ultrafast relaxation-related gain processes have been incorporated into FWM models to account for high conversion efficiency out to several terahertz [8]–[10] without accounting for gain asymmetry. While the effects of gain saturation and gain asymmetry due to cross-phase modulation type terms [7], [11] and pump and probe depletion have been considered, their role in the three saturation regimes, nonsaturating, moderately saturating, and strongly saturating, have not been compared.

In this paper, we present a detailed analytical and numerical analysis of FWM conversion efficiency based on a depleted pump and probe model that takes into account the effects of gain saturation, interband and intraband contributions to the nonlinear gain, power dependence of the coupling coefficients, and gain asymmetry. We show that for a certain range of parameter values, the conversion efficiency differs significantly from that given by the small-signal model. These deviations are due to gain asymmetry under low-level pump power and at small frequency detunings. Deviations from the small-signal model also occur under gain saturation conditions out to relatively large frequency detunings when pump and probe depletion and power dependence of the FWM coupling coefficients are accounted for. A general relationship is derived for a given amplifier that allows one to specify the range of amplifier saturated gain, input pump power, and frequency detuning, over which small-signal models are accurate.

Manuscript received April 15, 1996; revised June 24, 1996. This work was supported by the Air Force Office of Scientific Research (AFOSR) under Contract F49620-95-1-0024, a NSF National Young Investigator (NYI) Award, and a Subcontract from the University of Maryland.

The authors are with the Optical Communications and Photonics Network Laboratory, School of Electrical and Computer Engineering, Georgia Institute of Technology, Atlanta, GA 30332 USA.

Publisher Item Identifier S 0018-9197(96)07287-9.

II. Mixing Geometry and Coupled Wave Equations

We consider nondegenerate FWM frequency conversion in a traveling-wave SOA with collinearly injected pump and probe waves with z-dependent optical powers P_p and P_q and frequencies ω_p and ω_q, respectively. The FWM interaction between the pump and probe generates a signal wave at frequency $\omega_s = 2\omega_p - \omega_q$. The FWM signal at $2\omega_q - \omega_p$ is neglected, assuming that the probe power is much smaller than the pump power. Assuming the input waves are linearly polarized in the same direction, the quasi-steady-state evolution of the probe, pump, and signal wave amplitudes A_i, $i = q, p, s$ is given by the coupled equations

$$\frac{dA_q}{dz} = \frac{1}{2}\left[\{g(1-i\alpha)-\alpha_0\} - g\left(\eta_{qp}|A_p|^2 + \eta_{qs}|A_s|^2\right)\right]A_q - \frac{g}{2}\left[\eta_{ps}A_p^2A_s^*e^{-i\Delta kz}\right] \quad (1)$$

$$\frac{dA_p}{dz} = \frac{1}{2}\left[\{g(1-i\alpha)-\alpha_0\} - g\left(\eta_{pq}|A_q|^2 + \eta_{ps}|A_s|^2\right)\right]A_p - \frac{g}{2}\left[(\eta_{qp}+\eta_{sp})A_qA_sA_p^*e^{i\Delta kz}\right] \quad (2)$$

$$\frac{dA_s}{dz} = \frac{1}{2}\left[\{g(1-i\alpha)-\alpha_0\} - g\left(\eta_{sq}|A_q|^2 + \eta_{sp}|A_p|^2\right)\right]A_s - \frac{g}{2}\left[\eta_{pq}A_p^2A_q^*e^{-i\Delta kz}\right] \quad (3)$$

where $g(z) = g_0/(1+P(z)/P_s)$ is the saturated gain coefficient, g_0 is the small-signal gain coefficient, P_s and α are the saturation power and the linewidth enhancement factor of SOA induced by carrier density modulation, $P(z) = \sum_{i=q,p,s}|A_i(z)|^2$ is the total optical power inside the amplifier, and α_0 is the nonsaturable internal loss per unit length. We assume $\Delta k = 2k_2 - k_1 - k_3 \approx 0$ is satisfied due to the collinear geometry and low dispersion of the SOA [10].

Gain saturation due to self-phase modulation-type terms of the form $A_iA_iA_i^*$ and cross-phase modulation-type terms of the form $A_jA_iA_i^*, i \neq j$ are accounted for in (1)–(3). Gain asymmetry is also accounted for through terms of the form $A_iA_jA_i^*, i \neq j$ [11]. Higher order wave-mixing processes between the newly generated waves and the input waves have been neglected assuming the input pump power is strong compared to the input probe power.

The FWM coupling is described in the last terms of (1)–(3). The coefficients η_{ij} indicate the strength of index and gain gratings formed by beating between the associated waves A_i and A_j. The FWM coupling coefficient for the pump wave A_p has contributions from the scattering of probe by gratings formed by signal and pump and due to the scattering of signal by gratings formed by probe and pump waves. The complex coupling coefficients $\eta_{ij},\ i,j = q,p,s$, are given by

$$\eta_{ij}(z) = \frac{\left(\frac{1-i\alpha}{P_s}\right)}{1+\frac{P(z)}{P_s} - i(\omega_i-\omega_j)\tau_1} + \sum_{m=2}^{3}\frac{\left(\frac{1-i\alpha_m}{P_{sm}}\right)}{1-i(\omega_i-\omega_j)\tau_m}. \quad (4)$$

Equation (4) contains three relaxation-related gain mechanisms [10], carrier density modulation, carrier heating, and spectral hole burning. Phase interferences between multiple mechanisms cause an asymmetry in the mixing with respect to up- and down-conversion. The relaxation lifetimes are given by τ_m, $(m = 1,2,3)$ for carrier modulation, heating, and hole burning, respectively. The saturation powers P_{sm} and linewidth enhancement factors α_m are given for each process. The term $P(z)/P_s$ appears only in the denomenator of the carrier modulation contribution due to the extremely high saturation powers associated with carrier heating and spectral hole burning. The saturation powers for carrier heating and spectral hole burning are large due to fast relaxation times for these processes.

III. Small-Signal Model Analytical Solutions

In this section, we derive the small-signal model which assumes negligible influence on the FWM conversion efficiency due to pump and probe depletion and gain asymmetry. Under these approximations, the coupled equations (1)–(3) can be written as

$$\frac{dA_q}{dz} = \frac{1}{2}[g(1-i\alpha)-\alpha_0]A_q \quad (5)$$

$$\frac{dA_p}{dz} = \frac{1}{2}[g(1-i\alpha)-\alpha_0]A_p \quad (6)$$

$$\frac{dA_s}{dz} = \frac{1}{2}[g(1-i\alpha)-\alpha_0]A_s - \frac{1}{2}g\eta_{pq}A_p^2A_q^*. \quad (7)$$

Assuming that the FWM coupling coefficient η_{pq} is a constant independent of the total optical power inside the SOA, the field pump, probe, and signal amplitude exact solutions for (5)–(7), with $A_p(0)$, $A_q(0)$, and 0 as their input values, respectively, are

$$A_{p,q}(z) = A_{p,q}(0)e^{F(z)/2}e^{-\frac{i}{2}\alpha(F(z)+\alpha_0 z)} \quad (8)$$

$$A_s(z) = -\frac{1}{2}\eta_{pq}A_p^2(0)A_q^*(0)e^{F(z)/2}e^{-\frac{i}{2}\alpha(F(z)+\alpha_0 z)} \times\left[e^{F(z)} + \alpha_0\int_0^z e^{F(z')}dz' - 1\right] \quad (9)$$

where the function $F(z) = \int_0^z(g(z')-\alpha_0)dz'$. The SOA saturated gain G is $G = e^{F(L)}$, which is related to the unsaturated gain $G_0 = e^{g_0L}$ by

$$G = G_0e^{-F_0(L)} \quad (10)$$

where

$$F_0(L) = g_0\int_0^L \frac{P(z)/P_s}{1+P(z)/P_s}dz - \alpha_0L. \quad (11)$$

In the equations above, L is the length of the SOA.

At the amplifier output, the second bracketed term in (9) is equal to $[G + \alpha_0\int_0^L e^{F(z)}dz - 1]$. If the internal loss α_0 is low and the gain G is large, we can approximate this term by just the gain G. The signal intensity and FWM efficiency can then be written as

$$|A_s(L)|^2 \approx \left|\frac{1}{2}\eta_{pq}\right|^2 I_p^2(0)I_q(0)G^3 \quad (12)$$

$$\eta \approx \frac{|A_s(L)|^2}{I_q(0)} = \frac{1}{4}|\eta_{pq}|^2I_p^2(0)G^3. \quad (13)$$

Expressing η in dB, for the current set of assumptions, we obtain the same result derived in [10], shown as

$$\eta \approx 3G + 2I_p(0) + 20\log_{10}(|\eta_{pq}|/2) \quad (14)$$

where the SOA gain $G = 4.34F(L)$ in decibels, and the input pump power $I_p(0)$ is in dBm. Comparing (14) with (5) and (6) of [10], the complex constants c_m are given by

$$c_m = (1-i\alpha_m)/2P_{sm}. \quad (15)$$

As an example, using experimentally determined values of c_m given in [10], the linewidth enhancement factors α_m and the saturation powers P_{sm} corresponding to each of the three mechanisms can be estimated as: $\alpha = 3.6$, $\alpha_2 = -3.6$, $\alpha_3 = -24.5$, $P_s = 7.8$ mW, $P_{s2} = 0.69$ W, and $P_{s3} = 25.5$ W.

Note that P_{s2} and P_{s3} have large values compared to P_s because mechanisms 2 and 3 are ultrafast mechanisms compared to mechanism 1. The saturation power for any mechanism depends inversely on the lifetime associated with that mechanism [8].

A. The Influence of Probe Depletion on FWM Efficiency

The effect of probe depletion in the moderately to strongly saturating region is solved analytically by ignoring the pump depletion and the gain asymmetry terms in (1)–(3). Again, we assume that the FWM coupling coefficients η_{ps} and η_{pq} are constants independent of the total optical power inside the SOA (these constraints will be relaxed in numerical simulation section). The coupled wave equations are written as

$$\frac{dA_q}{dz} = \frac{1}{2}[g(1-i\alpha)-\alpha_0]A_q - \frac{1}{2}g\eta_{ps}A_p^2A_s^* \tag{16}$$

$$\frac{dA_p}{dz} = \frac{1}{2}[g(1-i\alpha)-\alpha_0]A_p \tag{17}$$

$$\frac{dA_s}{dz} = \frac{1}{2}[g(1-i\alpha)-\alpha_0]A_s - \frac{1}{2}g\eta_{pq}A_p^2A_q^*. \tag{18}$$

The exact solution of (16)–(18), with $A_q(0)$, $A_p(0)$, and 0 as the input values of probe, pump, and signal amplitudes, respectively, are

$$A_q(z) = A_q(0)e^{F(z)/2}e^{-\frac{i}{2}\alpha(F(z)+\alpha_0 z)} \times \cosh\left[\sqrt{C_1C_2^*}\left(e^{F(z)}+\alpha_0\int_0^z e^{F(z')}dz'-1\right)\right] \tag{19}$$

$$A_p(z) = A_p(0)e^{F(z)/2}e^{-\frac{i}{2}\alpha(F(z)+\alpha_0 z)} \tag{20}$$

$$A_s(z) = -A_q^*(0)\sqrt{\frac{C_2}{C_1^*}}e^{F(z)/2}e^{-\frac{i}{2}\alpha(F(z)+\alpha_0 z)} \times \sinh\left[\sqrt{C_1^*C_2}\left(e^{F(z)}+\alpha_0\int_0^z e^{F(z')}dz'-1\right)\right] \tag{21}$$

where $C_1 = \frac{1}{2}\eta_{ps}A_p^2(0)$ and $C_2 = \frac{1}{2}\eta_{pq}A_p^2(0)$. The function $F(z)$ in the above equations is defined after (9). The FWM conversion efficiency can be written as

$$\eta = \left|\frac{A_s(L)}{A_q(0)}\right|^2 = G\left|\frac{\eta_{pq}}{\eta_{ps}^*}\right|\left|\sinh\left[\frac{(\eta_{ps}^*\eta_{pq})^{1/2}}{2}|A_p(0)|^2\left(G+\alpha_0\int_0^L e^{F(z)}dz-1\right)\right]\right|^2. \tag{22}$$

If the complex arguments of the cosh and sinh functions in (19) and (21) are small so that $\cosh(x)\approx 1$ and $\sinh(x)\approx x$, then the above equations reduce to those given by (8) and (9), and (22) reduces to that given by (13) if the SOA's internal loss is low and gain is large. This condition can be specified by the relation

$$\frac{1}{\sqrt{2}}\left|\frac{(\eta_{ps}^*\eta_{pq})^{1/2}}{2}\right||A_p(0)|^2G \ll 1. \tag{23}$$

Equation (23) states that the probe depletion must be taken into account when the amplifier saturated gain is large, the input pump power is large, and/or the pump-probe detuning is small. Equation (23) serves as a test as to when probe depletion accounts for deviation from the small-signal model result given by (14).

IV. Numerical Simulation

In this section, pump and probe depletion, gain asymmetry, and power dependence of coupling coefficients are accounted for by solving the coupled wave equations numerically. These results are compared to those obtained using the small-signal model in (14) and with results not including gain asymmetry.

Equations (1)–(3) are solved numerically by assuming that the SOA's nonsaturable internal loss per unit length is small compared to its gain and can be neglected, i.e., $\alpha_0 = 0$. Gain asymmetry and the power dependence of η_{ij} are accounted for by retaining $P(z)/P_s$ in the denominator of the first term of (4). In our simulations, we have used the values $\tau_1 = 200$ ps, $\tau_2 = 650$ fs, $\tau_3 = 50$ fs, $c_1 = 0.24\exp(-i1.30)$, $c_2 = 0.0027\exp(i1.30)$, and $c_3 = 0.000\,48\exp(i1.53)$ given in [10].

Figs. 1–9 show how various parameters influence the predicted conversion efficiency, η, using the small-signal model (dashed lines) and exact solutions (dotted and solid lines). The solid lines are simulation results from the full system of equations and the dotted lines show the effect of removing gain asymmetry from the simulation. We performed simulations for up-conversion, i.e., $\Delta\nu = (\omega_p - \omega_q)/2\pi < 0$, and down-conversion, i.e., $\Delta\nu > 0$. The FWM down-conversion efficiency is slightly larger than the up-conversion efficiency. However, the qualitative behavior for both up- and down-conversion is similar. In the simulations, the small-signal gain G_0 was limited from 10 dB to 35 dB.

At higher pump powers, the FWM efficiency calculated by the small-signal model deviate significantly from the numerical simulation results. The dependency of the conversion efficiency on the saturated gain G for four different pump powers P_p is illustrated in Fig. 1. Here, the detuning is $\Delta\nu = -10$ GHz and the probe power is $P_q = -30$ dBm. We see that for a pump power of $P_p = 0.5$ mW, the efficiency deviates about 2 dB, and for $P_p = 10$ mW this deviation becomes 6 dB. Note that the deviation is relatively insensitive to changes in the saturated gain G itself and still closely follows the small-signal G^3 dependence. The maximal deviation for $P_p = 10$ mW is only about 1.5 dB larger than the minimal deviation.

For constant pump power, the gain dependence of η and its deviation from the small-signal model is relatively insensitive to variations of probe power. Fig. 2 shows the conversion efficiency η as a function of saturated gain for constant pump power $P_p = 10$ dBm, detuning $\Delta\nu = -10$ GHz and for probe powers $P_q = -30$ dBm, -20 dBm, and -10 dBm. For all three values of probe power, the curves for the full system of equations (solid curves) are identical, the curves for the simulation without gain asymmetry (dotted curves) are identical, and the curves for the small-signal analysis (dashed curves) are also identical. The deviation between simulation and small-signal analysis is larger than 5 dB, and the deviation

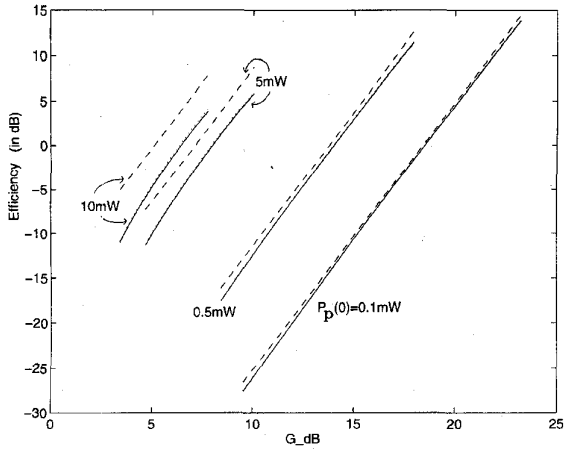

Fig. 1. FWM frequency conversion efficiency as a function of SOA saturated gain for input pump powers $P_p = 0.1$ mW, 0.5 mW, 5 mW, and 10 mW. Input probe power is $P_q = -30$ dBm and pump-probe detuning frequency is $\Delta\nu = -10$ GHz. The dashed curves are obtained by using (14), dotted curves are obtained by solving (1)–(3) without gain asymmetry terms, and solid curves include gain asymmetry. The solid and dotted curves take into account power dependence of coupling coefficients.

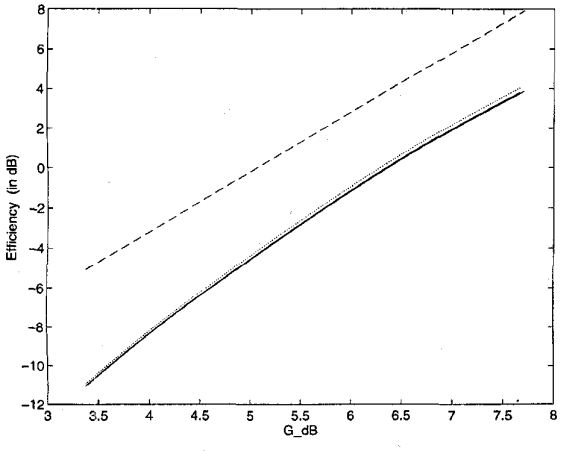

Fig. 2. FWM frequency conversion efficiency as a function of SOA saturated gain for input probe powers $P_q = -30$ dBm, -20 dBm, and -10 dBm, input pump power $P_p = 10$ dBm, and pump-probe detuning frequency $\Delta\nu = -10$ GHz. Dashed curves from (14), dotted curves from (1)–(3) without gain asymmetry terms, and solid curves with gain asymmetry.

between neglecting gain asymmetry and the full system of equations is about 0.1 dB.

In Fig. 3, the pump-to-probe power ratio is kept constant at $P_p/P_q = 30$ dB. For the input pump power $P_p = 0$ dBm and input probe power $P_q = -30$ dBm, the maximal deviation is about 2 dB, and for $P_p = 10$ dBm and $P_q = -20$ dBm, the maximal deviation is 7 dB.

Frequency detuning $\Delta\nu$ also plays an important role, as illustrated in Fig. 4. The conversion efficiency is plotted as a function of saturated gain G for different input pump and probe powers, keeping their ratio constant as in Fig. 3, and a detuning $\Delta\nu = -1$ THz. Comparison with Fig. 3 shows that smaller detuning increases the deviation in conversion efficiency. For example, for $P_p = 10$ dBm, the maximal

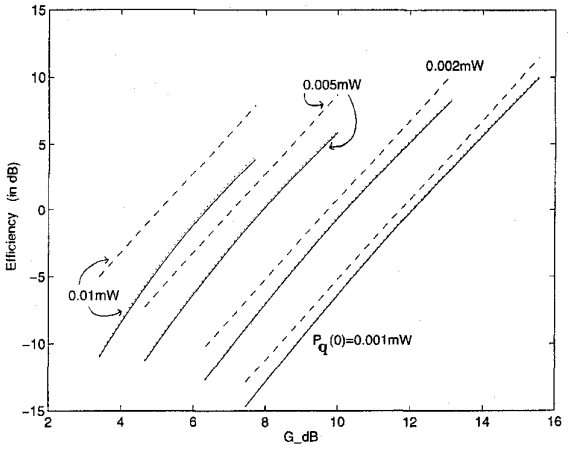

Fig. 3. FWM frequency conversion efficiency as a function of SOA saturated gain for input pump-probe power ratio $P_p/P_q = 30$ dB, input pump powers $P_p = 1$ mW, 2 mW, 5 mW, and 10 mW, and pump-probe detuning frequency $\Delta\nu = -10$ GHz. Dashed curves from (14), dotted curves from (1)–(3) without gain asymmetry terms, and solid curves with gain asymmetry.

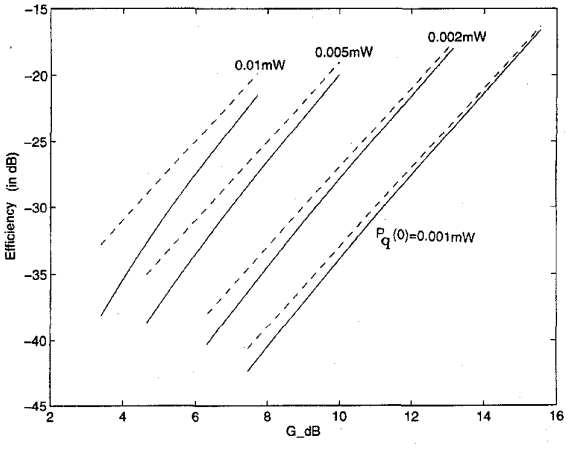

Fig. 4. FWM frequency conversion efficiency as a function of SOA saturated gain for input pump-probe power ratio $P_p/P_q = 30$ dB, input pump powers $P_p = 1$ mW, 2 mW, 5 mW, and 10 mW, and pump-probe frequency detuning $\Delta\nu = -1$ THz. Dashed curves from (14), dotted curves from (1)–(3) without gain asymmetry terms, solid curves with gain asymmetry.

deviation for $\Delta\nu = -1$ THz is 5 dB, and for $\Delta\nu = -10$ GHz it is 7 dB. This result illustrates an overestimate of the conversion efficiency using the small-signal gain model for detuning out to 1 THz.

The change in deviation between the small-signal model and the full model for different detunings is investigated in further detail in Fig. 5. The conversion efficiency η is plotted as a function of saturated gain G. Pump and probe powers are kept constant at $P_p = 10$ dBm and $P_q = -30$ dBm, for various values of detuning $\Delta\nu$. For detuning $\Delta\nu = 1$ THz, the results from the simulation with and without gain asymmetry coincide. With decreasing detuning, the deviation between the small-signal model and the full simulation model increases, e.g., for $G = 7$ dB and $\Delta\nu = 1$ THz, the deviation is 2 dB, for $\Delta\nu = 10$ GHz, the deviation is 4 dB.

Based on Figs. 1–5, the two factors which determine the deviation from small-signal model and the full system of

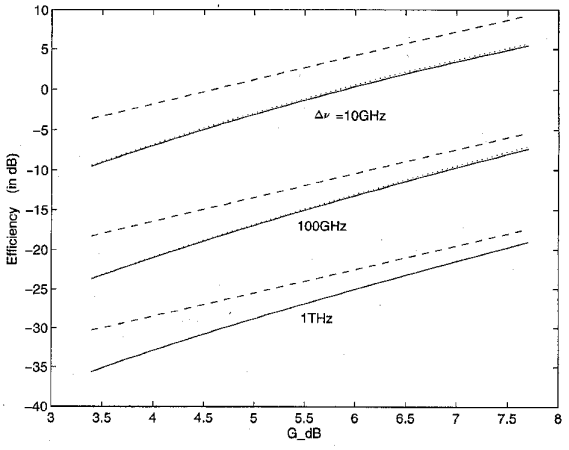

Fig. 5. FWM frequency conversion efficiency as a function of SOA saturated gain for input pump and probe powers $P_p = 10$ dBm and $P_q = -30$ dBm, respectively, and pump-probe frequency detunings $\Delta\nu = 10$ GHz, 100 GHz, and 1 THz. Dashed curves from (14), dotted curves from (1)–(3) without gain asymmetry terms, solid curves with gain asymmetry.

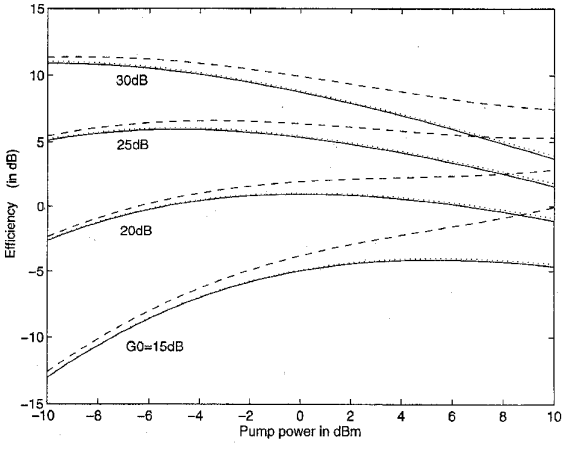

Fig. 6. FWM frequency conversion efficiency as a function of input pump power P_p for unsaturated gain $G_0 = 15$ dB, 20 dB, 25 dB, and 30 dB. Input probe power is $P_q = -30$ dBm and pump-probe frequency detuning is $\Delta\nu = 10$ GHz. Dashed curves from (14), dotted curves from (1)–(3) without gain asymmetry terms, solid curves with gain asymmetry.

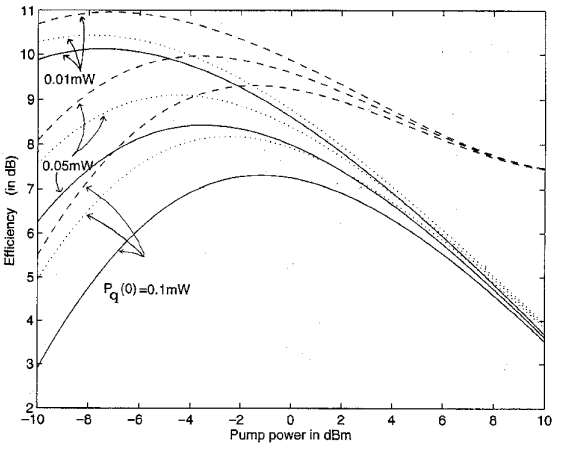

(a)

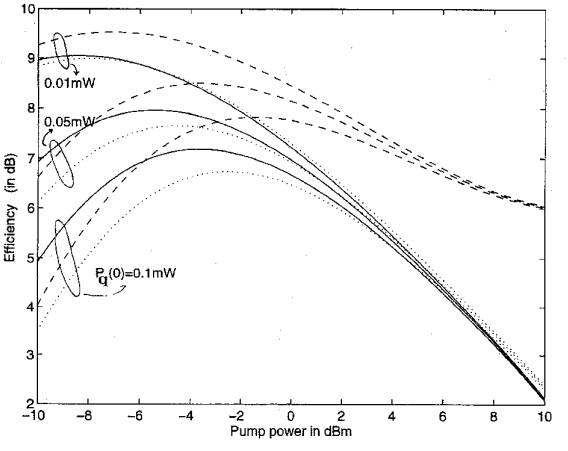

(b)

Fig. 7. FWM frequency conversion efficiency as a function of input pump power P_p for unsaturated gain $G_0 = 30$ dB and input probe powers $P_q = 0.01$ mW, 0.05 mW, and 0.1 mW. Dashed curves from (14), dotted curves from (1)–(3) without gain asymmetry terms, solid curves with gain asymmetry: a) Pump-probe frequency detuning $\Delta\nu = 10$ GHz, and b) pump-probe frequency detuning $\Delta\nu = -10$ GHz.

equations are pump power and frequency difference between pump and probe. The remaining figures verify this result in more detail.

Keeping the probe power at a small constant value and for constant detuning, the deviation of the conversion efficiency varies significantly with pump power. In Fig. 6, starting at small pump powers of $P_p = -10$ dBm, all models accurately predict η. This is not true for larger input pump powers. At approximately $P_p = -4$ dBm, we start seeing increasingly larger deviations of the conversion efficiency η calculated using the small-signal model. Interestingly, this deviation increases with decreasing small-signal gain G_0, and the deviation of the conversion efficiency due to gain asymmetry does not change significantly with change in pump power or change in small-signal gain. This points to gain saturation as dominant effect.

For very small pump powers, i.e., $P_p < 0$ dBm, the deviation of the conversion efficiencies η increases with increasing probe power. Fig. 7 shows the deviation in conversion efficiency for large unsaturated gain $G_0 = 30$ dB. In Fig. 7(a), the detuning is $\Delta\nu = 10$ GHz, and in Fig. 7(b), the detuning is $\Delta\nu = -10$ GHz. Up to a pump power of $P_p = 0$ dBm, the deviation of the dashed and the dotted lines from the solid lines is sensitive to probe power. The deviation becomes independent of probe power for pump powers larger than 6 dBm. Note that in Fig. 7(b), for low-pump and low-probe powers, the small-signal model and the simulation without including gain asymmetry predict lower efficiencies than the full simulation model. When deriving the equations, we assumed that the pump power is much larger than the probe power. In the low-pump/high-probe power region of Fig. 7(a) and (b), this assumption has been violated. We performed the simulations with a full system of four waves, and in the worst

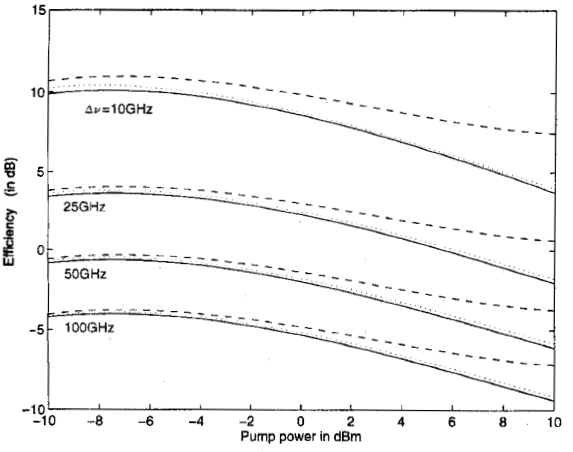

Fig. 8. FWM frequency conversion efficiency as a function of input pump power P_p for unsaturated gain $G_0 = 30$ dB, input probe power $P_q = -20$ dBm, and pump-probe frequency detuning $\Delta\nu = 10$ GHz, 25 GHz, 50 GHz, and 100 GHz. Dashed curves from (14), dotted curves from (1)–(3) without gain asymmetry terms, solid curves with gain asymmetry.

case the resulting efficiencies deviate less than 1 dB from the results in Fig. 7(a) and (b).

Fig. 8 shows that even for large detunings, there is still a large deviation of the conversion efficiency at high-input pump powers. For detunings between $\Delta\nu = 10$ GHz and 100 GHz and pump powers between $P_p = -10$ dBm and 10 dBm, the deviation in conversion efficiency increases with decreasing frequency detuning and increasing pump power. For very low detuning, i.e., detuning below 10 GHz, the effect of gain asymmetry is very strong. Fig. 9 shows the conversion efficiency for detuning down to $\Delta\nu = 1$ GHz. Up-conversion is shown in Fig. 9(a), and Fig. 9(b) shows down-conversion. Using a constant large-input pump power $P_p = 10$ dBm and a small constant probe power $P_q = -20$ dBm, the influence of the frequency difference becomes very pronounced, particularly below $\Delta\nu = 10$ GHz. For a small-signal gain $G_0 = 30$ dB, the deviation between the small-signal model and the full model changes from about 4 dB at $\Delta\nu = 10$ GHz to 17 dB at $\Delta\nu = 1$ GHz.

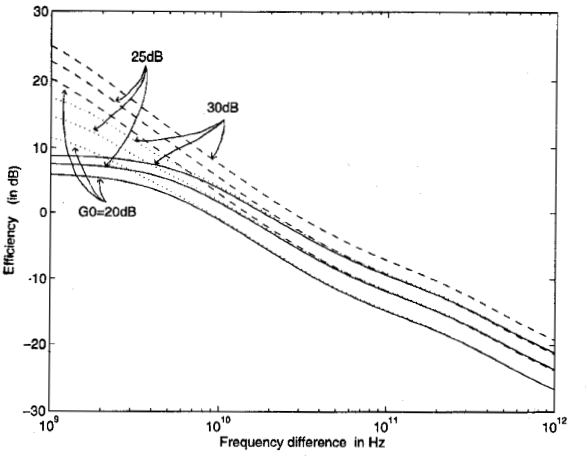

(a)

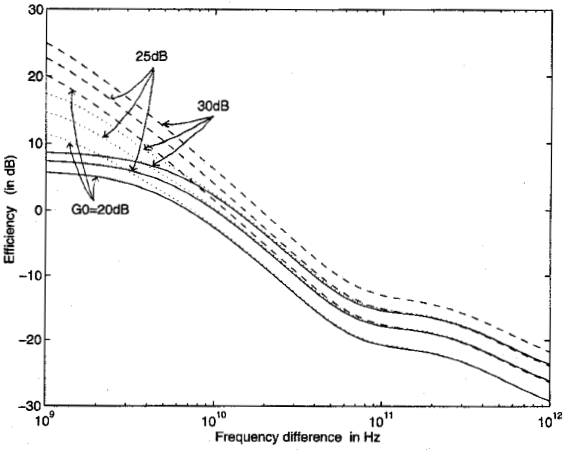

(b)

Fig. 9. FWM frequency conversion efficiency as a function of pump-probe frequency detuning for unsaturated gain $G_0 = 20$ dB, 25 dB, and 30 dB. Input pump and probe powers are $P_p = 10$ dBm and $P_q = -20$ dBm, respectively. Dashed curves from (14), dotted curves from (1)–(3) without gain asymmetry terms, solid curves with gain asymmetry: a) down-conversion and b) up-conversion.

V. Summary and Conclusion

We have studied the influence of pump-probe depletion, power dependence of coupling coefficients, and gain asymmetry on nondegenerate four-wave mixing efficiency in semiconductor optical amplifiers. Our model takes into account gain saturation and ultrafast gain mechanisms. The coupled wave equations are solved analytically for two different cases: 1) depletion of both pump and probe are neglected, and 2) depletion of pump is neglected but that of probe is taken into account. These cases assume that the effects of gain asymmetry and power dependence of coupling coefficients are small and can be ignored. The third case where depletion of both pump and probe waves together with gain asymmetry and power dependence of coupling coefficients are incorporated is solved numerically. The analytical solutions of the wave equations for the cases 1) and 2) enable us to obtain bounds on the conversion efficiency. These bounds suggest that small-signal model is valid only if the input pump power is small, the saturated gain G is small, and/or the pump-probe detuning is large.

Numerical results presented for various parameter ranges of the SOA for the case 3) confirm the validity of these findings. For large pump powers, the small-signal model predicts too optimistic conversion efficiencies. However, it is not necessary to include gain asymmetry in the model as long as the frequency-detuning is high to moderate. For small frequency detuning, i.e., $\Delta\nu < 10$ GHz, and for small pump powers in combination with large probe powers, gain asymmetry can no longer be neglected. We believe that deviations in frequency-conversion efficiency between various models in this operating region of the SOA are due to the combined effects of pump-probe depletion and power dependence of coupling coefficients. Finally, it should be important to perform calculations with different values of α, P_s, and τ. We will report these results in a separate publication.

ACKNOWLEDGMENT

The authors acknowledge the assistance of C. Scholz in preparing the manuscript and verifying part of the results in Fig. 7, using a full system of four-wave equations.

REFERENCES

[1] R. Schnabel, U. Hilbk, T. Hermes, P. Meibner, C. Helmolt, K. Magari, F. Raub, W. Pieper, F. J. Westphal, R. Ludwig, L. Kuller, and H. G. Weber, "Polarization insensitive frequency conversion of a 10-channel OFDM signal using four-wave-mixing in a semiconductor laser amplifier," *IEEE Photon. Technol. Lett.*, vol. 6, pp. 56–58, Jan. 1994.

[2] J. P. R. Lacey, S. J. Madden, M. A. Summerfield, R. S. Tucker, and A. I. Paris, "Four-channel WDM optical phase conjugator using four-wave mixing in a single semiconductor optical amplifier," *Electron. Lett.*, vol. 31, pp. 743–744, Apr. 1995.

[3] S. Murata, A. Tomita, J. Shimizu, M. Kitamura, and A. Suzuki, "Observation of highly nondegenerate four-wave mixing ($\geq$1 THz) in an InGaAsP multiple quantum well laser," *Appl. Phys. Lett.*, vol. 58, pp. 1458–1460, Apr. 1991.

[4] S. Murata, A. Tomita, J. Shimizu, and A. Suzuki, "THz optical-frequency conversion of 1 Gb/s-signals using highly nondegenerate four-wave mixing in an InGaAsP semiconductor laser," *IEEE Photon. Technol. Lett.*, vol. 3, pp. 1021–1023, Nov. 1991.

[5] J. Zhou, N. Park, K. J. Vahala, M. A. Newkirk, and B. I. Miller, "Broadband wavelength conversion with amplification by four-wave mixing in semiconductor traveling-wave amplifiers," *Electron. Lett.*, vol. 30, pp. 859–860, May 1994.

[6] A. D'Ottavi, E. Iannone, A. Mecozzi, S. Scotti, P. Spano, R. Dall'Ara, J. Eckner, and G. Guekos, "Efficiency and noise performance of wavelength converters based on FWM in semiconductor optical amplifiers," *IEEE Photon. Technol. Lett.*, vol. 7, pp. 357–359, Apr. 1995.

[7] T. Mukai and T. Saitoh, "Detuning characteristics and conversion efficiency of nearly degenerate four-wave mixing in a 1.5-μm traveling-wave semiconductor laser amplifier," *IEEE J. Quantum Electron.*, vol. 26, pp. 865–875, May 1990.

[8] G. P. Agrawal, "Population pulsations and nondegenerate four-wave mixing in semiconductor lasers and amplifiers," *J. Opt. Soc. Amer. B*, vol. 5, pp. 147–159, Jan. 1988.

[9] K. Kikuchi, M. Kakui, C. E. Zah, and T. P. Lee, "Observation of highly nondegenerate four-wave mixing in 1.5 μm traveling-wave semiconductor optical amplifiers and estimation of nonlinear gain coefficient," *IEEE J. Quantum Electron.*, vol. 28, pp. 151–156, Jan. 1992.

[10] J. Zhou, N. Park, J. W. Dawson, K. J. Vahala, M. A. Newkirk, and B. I. Miller, "Efficiency of broadband four-wave mixing wavelength conversion using semiconductor traveling-wave amplifiers," *IEEE Photon. Technol. Lett.*, vol. 6, pp. 50–52, Jan. 1994.

[11] T. E. Darcie and R. M. Jopson, "Nonlinear interactions in optical amplifiers for multifrequency lightwave systems," *Electron. Lett.*, pp. 638–640, May 1988.

N. C. Kothari, photograph and biography not available at the time of publication.

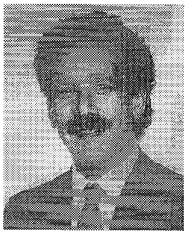

Daniel J. Blumenthal (S'91–M'93) received the B.S.E.E. degree from the University of Rochester, NY, in 1981, the M.S.E.E. degree from Columbia University, New York, NY, in 1988, and the Ph.D. degree from the University of Colorado at Boulder in 1993.

In 1981 he joined StorageTek, Louisville, CO, where he was engaged in research and development in optical data storage systems. In 1986, he worked at Columbia University as a research engineer in the areas of photonic switching systems and ultrafast all-optical networks and signal processing. In 1990, he worked as a Graduate Research Assistant on multiwavelength photonic-switched interconnects for distributed computing applications. Presently, he is an Assistant Professor in the School of Electrical and Computer Engineering at the Georgia Institute of Technology, Atlanta, and heads the Optical Communications and Photonic Networks (OCPN) Research Group. His current research areas are in optical communications, wavelength division multiplexing, photonic-switched and all-optical networking, wavelength conversion in semiconductor devices, and optical information processing. He has authored or co-authored over 25 papers in these and related areas. He is currently an Associate Editor for the IEEE TRANSACTIONS ON COMMUNICATIONS in the optical communication area.

Dr. Blumenthal is a member of the Optical Society of America and the IEEE Lasers and Electro-Optic Society (LEOS), and he is also Chair of the LEOS Atlanta Chapter and serves on the program committee for the 1997 Conference on Optical Fiber Communications (OFC). He is recipient of an NSF Young Investigator Award.